

# Chapter 11

## Novel $\gamma$ -Butyrolactone Derivatives as Muscarinic Receptor Antagonists: Pharmacophore Elucidation and Docking Analyses

Richie R. Bhandare, Rong Gao, Daniel J. Canney  
and Prashant S. Kharkar

**Abstract** Our efforts in design and development of novel muscarinic acetylcholine receptor (mAChR) antagonists led to the development of a novel series of  $\gamma$ -butyrolactone derivatives. We were interested in understanding the contributions of the structural features of these molecules for receptor affinity and subtype selectivity, if any, to guide further design of second-generation analogs with tailor-made potency and selectivity. Initially, 3D pharmacophore hypotheses were developed using high affinity M1 and M2 antagonist ligands. The ‘extended’ and ‘compact’ hypotheses were then used for the retrospective virtual screening of the  $\gamma$ -butyrolactone derivatives. Further, these molecules were then docked into the M2 receptor orthosteric binding site. The results obtained from the pharmacophore- and structure-based investigations were in agreement with the structure–activity relationship (SAR) observations. The key findings of these studies will be helpful for further design and development of subtype-selective muscarinic receptor ligands.

**Keywords** Muscarinic receptors ·  $\gamma$ -butyrolactones · Pharmacophore search · Orthosteric binding site

---

R.R. Bhandare · P.S. Kharkar (✉)  
SPP School of Pharmacy and Technology Management, SVKM’s NMIMS,  
V.L. Mehta Road, Vile Parle (West), Mumbai 400056, India  
e-mail: prashant.kharkar@nmims.edu

R.R. Bhandare  
e-mail: richiebhandare@gmail.com

R.R. Bhandare · R. Gao · D.J. Canney  
Department of Pharmaceutical Sciences, School of Pharmacy,  
Moulder Center for Drug Discovery Research, Temple University,  
3307 N. Broad Street, Philadelphia, PA 19140, USA  
e-mail: psgaopsgao@gmail.com

D.J. Canney  
e-mail: canney@temple.edu

## 11.1 Introduction

The cholinergic neurotransmitter acetylcholine (ACh) binds nonselectively to its receptors, namely, muscarinic and nicotinic, thereby regulating a wide variety of functions peripherally and centrally, depending on their location [1–3]. The muscarinic ACh receptors (mAChRs) are classified into five subtypes, M1–M5, which belong to the Family A of G-protein-coupled receptor (GPCR) super family. Molecular cloning studies have identified the existence of these molecularly distinct mammalian mAChR subtypes. In general subtypes M1, M3, and M5 are positively coupled to Gq/11 class of G proteins, whereas M2 and M4 subtypes are negatively coupled to Gi/o class. Given their wide distribution (centrally and peripherally) and involvement in crucial functions, mAChRs are targets for drug discovery efforts for many diseases and disorders such as Alzheimer's disease, chronic obstructive pulmonary disease (COPD), urinary incontinence, schizophrenia and diabetes [4, 5].

Until recently, the efforts to develop subtype-selective ligands for the mAChRs have been hampered due to the lack of X-ray crystal structures of the membrane bound proteins and their high degree of homology among the receptor subtypes [6, 7]. In the last couple of years, the deposition of antagonist-bound crystal structures of human M2 [8] and rat M3 [9] receptors in Protein Data Bank (PDB) rejuvenated the mAChR ligand design (orthosteric and allosteric) field [10, 11]. The release of agonist-bound crystal structures (with and without allosteric modulator) of the human M2 receptor in 2013 initiated a new chapter in this research area [12]. Numerous studies involving homology modeling and virtual screening using molecular docking of the mAChR ligands have been reported [13]. Similar to the structure-based design efforts, the ligand-based strategies such as pharmacophore elucidation have been used for the design of selective mAChR ligands [14]. Thus, the design and development of selective mAChR agonists and antagonists is an intensive area of research.

To understand the selectivity of the ligands towards different subtypes, homology modeling and molecular docking analysis of ACh in all mAChRs have been investigated to reveal unique interactions between the native ligand and the binding pockets of M1–M5 receptors [15]. The study reported various interactions of ACh within the orthosteric binding pocket of each of the five muscarinic subtypes. For example, binding of ACh to the M1 receptor is mediated by (a) H-bonding interactions of the ester group with Thr192 (TM5) and Asn382 (TM6), (b) electrostatic interaction of the quaternary ammonium group with Asp105 (TM3), and (c) hydrophobic interactions in the receptor pocket. The binding of the aromatic residues constituting auxiliary binding may contribute to the higher affinity but have not guided modulation of subtype selectivity of the muscarinic ligands [16]. Similar residues involved in the interaction of ACh in the orthosteric binding sites of M1–M5 receptors were also found to interact with the agonists and antagonists in the M1–M3 receptor models [17–19]. Overall, careful tinkering of the aromatic/hydrophobic features in the ligands may lead to mAChR subtype selectivity.

Our early interest in designing novel mAChR ligands has led to preceding studies detailing the identification of substituted lactones as lead muscarinic compounds using an approach previously reported by Kaiser et al. [20]. The authors had applied the principle of increasing conformational rigidity in a lead in an attempt to retain or improve affinity and improve subtype selectivity [21]. Using a known nonselective muscarinic antagonist (**1**, Fig. 11.1) as lead compound, a series of constrained analogs of benactyzine were designed, synthesized and tested as muscarinic ligands. The biphenyl lactones with an N-substituted imidazole ring led to the discovery of **2** as M3 antagonist [22]. Several of these compounds were identified as potential leads for the development of drugs for urinary incontinence. Replacement of both the phenyl rings in **2** with ethyl groups (**3**, Fig. 11.1) resulted in agonist activity in M1 reciprocal hindlimb scratching assay [22].

The lactones in the present investigation were designed based on the preliminary binding data, structure-activity relationship (SAR) studies and sub-structures present in the reported ligands. An important distinction between the newly designed ligands (Fig. 11.2) and the lead lactones (Fig. 11.1) is the presence of (un)substituted aryl group that provides additional opportunities for interactions with auxiliary binding sites of the mAChRs.

Preliminary binding studies conducted at CEREP revealed that an ethylene linker was better than a methylene linker. Another observation was the effect of ortho substitution on the aryl ring showing improved percentage inhibition values

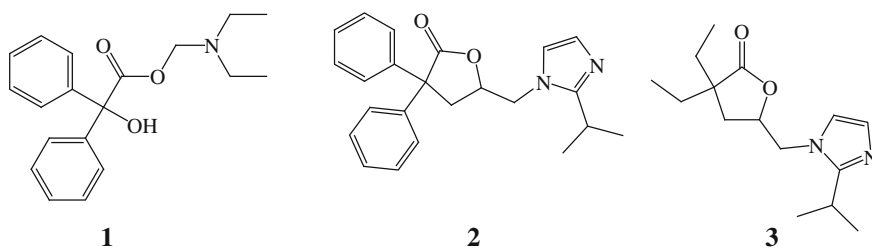


Fig. 11.1 Design strategy based on benactyzine (**1**) and initial lead structures (**2** and **3**)

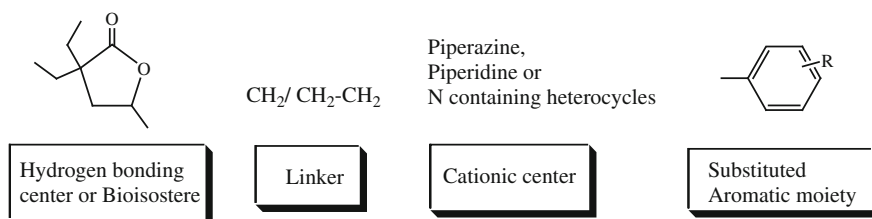


Fig. 11.2 Structural features of the newly designed ligands

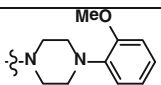
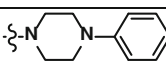
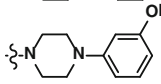
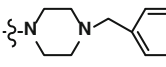
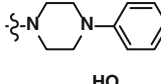
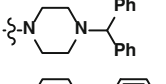
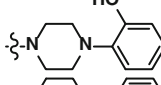
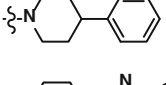
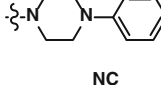
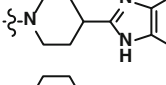
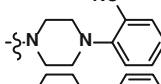
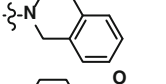
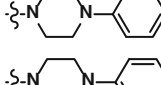
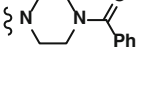
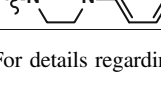
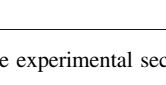
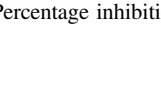





over meta- and para substitutions. SAR data suggest that steric and electronic influences were minimal in this preference for meta substituents. The improved binding might be the result of increased length of the flexible molecule and the resulting position of substituents on the aromatic ring [19, 20]. The present study reviews the preliminary evaluation of these novel ligands in binding assays and in subtype selectivity assays followed by elucidation of 3D pharmacophore models. The models are based on M1- and M2-preferring antagonists followed by docking analyses in the M2 orthosteric binding site in an attempt to further investigate the mAChR binding affinity and if possible, selectivity of these muscarinic antagonists.

## 11.2 Methodology

### 11.2.1 Chemistry

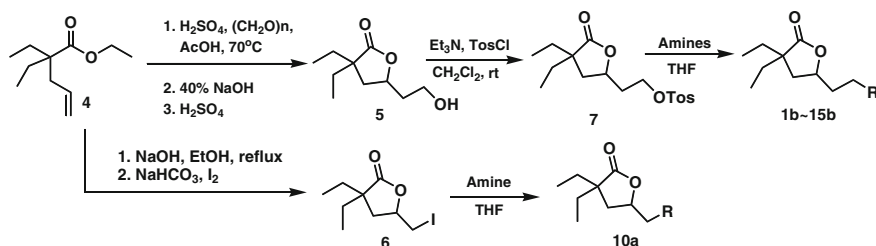
The newly designed lactone-based compounds **1a/1b-15a/15b** (Table 11.1) have been published previously [22]. Scheme 11.1 shows the synthesis of a methylene and ethylene series of lactone-based muscarinic ligands beginning with the olefinic ester starting material.

**Table 11.1** Preliminary binding data for compounds **1a-15a** and **1b-15b**

R	#	n	% inhib <sup>1,2</sup>	R	#	n	% inhib <sup>1,2</sup>
	<b>1a</b>	1	32		<b>9a</b>	1	16
	<b>1b</b>	2	82		<b>9b</b>	2	74
	<b>2a</b>	1	9		<b>10a</b>	1	28
	<b>2b</b>	2	75		<b>10b</b>	2	63
	<b>3a</b>	1	26		<b>11a</b>	1	97
	<b>3b</b>	2	56		<b>11b</b>	2	99
	<b>4a</b>	1	46		<b>12a</b>	1	68
	<b>4b</b>	2	81		<b>12b</b>	2	86
	<b>5a</b>	1	7		<b>13a</b>	1	46
	<b>5b</b>	2	61		<b>13b</b>	2	66
	<b>6a</b>	1	31		<b>14a</b>	1	44
	<b>6b</b>	2	83		<b>14b</b>	2	57
	<b>7a</b>	1	18		<b>15a</b>	1	5
	<b>7b</b>	2	57		<b>15b</b>	2	33
	<b>8a</b>	1	18				
	<b>8b</b>	2	70				

<sup>1</sup>For details regarding the evaluation of results, see experimental section

<sup>2</sup>Percentage inhibition at 10  $\mu$ M



**Scheme 11.1** Synthesis of a homologous series of lactone-based muscarinic ligands **10a**, **1b-15b**

## 11.2.2 Molecular Modeling

### 11.2.2.1 Hardware and Software

All the molecular modeling studies described herein were performed on Lenovo UltraBook Laptop (Intel<sup>®</sup> Core™ i5-3317U CPU @ 1.70 GHz, RAM 4 GB) running Windows 7 Home Basic Operating System. Schrödinger Small-Molecule Drug Discovery Suite Release 2013-1 [23] and the products included therein were used for various molecular modeling operations.

### 11.2.2.2 3D Pharmacophore Elucidation

Phase, version 3.5 [24] as implemented in Schrödinger Suite 2013-1, was used for developing common pharmacophore hypotheses.

### 11.2.2.3 Data Set

Table 11.2 lists all the M1- and M2-preferring antagonists along with their mAChR binding profiles used in the present investigations. The structures of the entire data set molecules are shown in Chart 11.1. Compounds **8-13** were used for M1, whereas **9, 14-18** were used for M2 pharmacophore elucidation. The compounds were selected based on their  $\text{pK}_i$  values for M1-M5 subtypes. Structural diversity was the main criterion for inclusion of the molecules in the data set.

The molecular structures of the antagonists were built from SMILES strings using 2D Sketcher functionality in Maestro, version 9.4 [25]. The 3D structures were prepared using LigPrep, version 2.6 [26], using default settings. These structures were then imported and subjected to the pharmacophore model development process. Additional conformations were enumerated in the 'Prepare Ligands' step as implemented in Phase, version 3.5. The common pharmacophoric features were searched followed by scoring of the hypotheses. The scoring process

**Table 11.2** Biological activities of muscarinic receptor antagonists used in the present investigation<sup>a</sup>

Compound No.	pK <sub>i</sub>					Glide XP GScore
	M1	M2	M3	M4	M5	3UON
<b>8</b> ( <i>R</i> -Trihexylphenidyl)	9.43	8.15	8.61	9.08	8.3	-13.214
<b>9</b> (Atropine) <sup>b</sup>	8.5–9.6	7.8–9.2	8.9–9.8	8.7–9.5	9.3–9.7	-13.478
<b>10</b> (Darifenacin) <sup>b</sup>	8.3	7.3–7.6 <sup>c</sup>	9.1	8.1	8.6	-5.622
<b>11</b> (Proprantheline) <sup>b</sup>	9.7	9.5	10.0	10.2	–	-12.663
<b>12</b> (4-DAMP) <sup>b</sup>	9.2	8.3	9.3	8.9	9.0	-12.670
<b>13</b> (Pirenzepine)	8.20	6.65	6.86	7.43	7.05	-5.803
<b>14</b> (AF-DX 384)	7.51	8.22	7.18	8.0	6.27	-9.222
<b>15</b> (AQ-RA 741)	7.54	8.37	7.20	8.19	6.08	-7.372
<b>16</b> (Dexetimide) <sup>b</sup>	–	8.9	–	–	–	-12.774
<b>17</b> ( <i>S</i> -Dimethindene)	7.08	7.78	6.70	7.0	–	-10.125
<b>18</b> (Himbacine)	6.97	8.0	7.03	7.96	6.31	-11.516

<sup>a</sup>Receptor binding potencies determined against human receptors

<sup>b</sup>The binding potency values are taken from IUPHAR database

<sup>c</sup>Inverse agonist

leads to identification of the best candidate hypothesis with overall ranking of all the hypotheses. The scoring algorithm in phase considers the alignment of site points and vectors, selectivity, volume overlap, number of ligands matched, relative conformations energy and activity [27]. The hypotheses thus obtained were clustered and the top-scoring members of top five clusters were inspected. The selection of the best hypothesis was based on alignment score, volume score, and selectivity. All the hypotheses contained three features—acceptor (A), positive-ionizable (P) and ring (R). These features represent the key binding interactions of the antagonists with the muscarinic receptors as seen from the docked poses and are described in detail in Sect. 11.3. The top-scoring hypotheses were further used for retrospective virtual screening of the lactone derivatives (**1a-15a** and **1b-15b**, Table 11.2) to check if they shared these features at appropriate pharmacophoric distances. This exercise was aimed at obtaining useful information for guiding design of novel lactone derivatives as muscarinic antagonists and also, to prioritize the current series for further SAR exploration.

#### 11.2.2.4 Docking Studies

Glide, version 5.9 [28] was used for all the docking studies described in the present work. PDB search of muscarinic receptors (performed on January 13, 2014) resulted in 4 hits—three M2 and one M3 structures. Two of the human M2 receptor structures bound to an agonist with/without an allosteric modulator (PDB IDs 4MQT and 4MQS, respectively) were released only in November 2013 [12]. The lone human M2 receptor structure bound to an antagonist (PDB ID 3UON) was

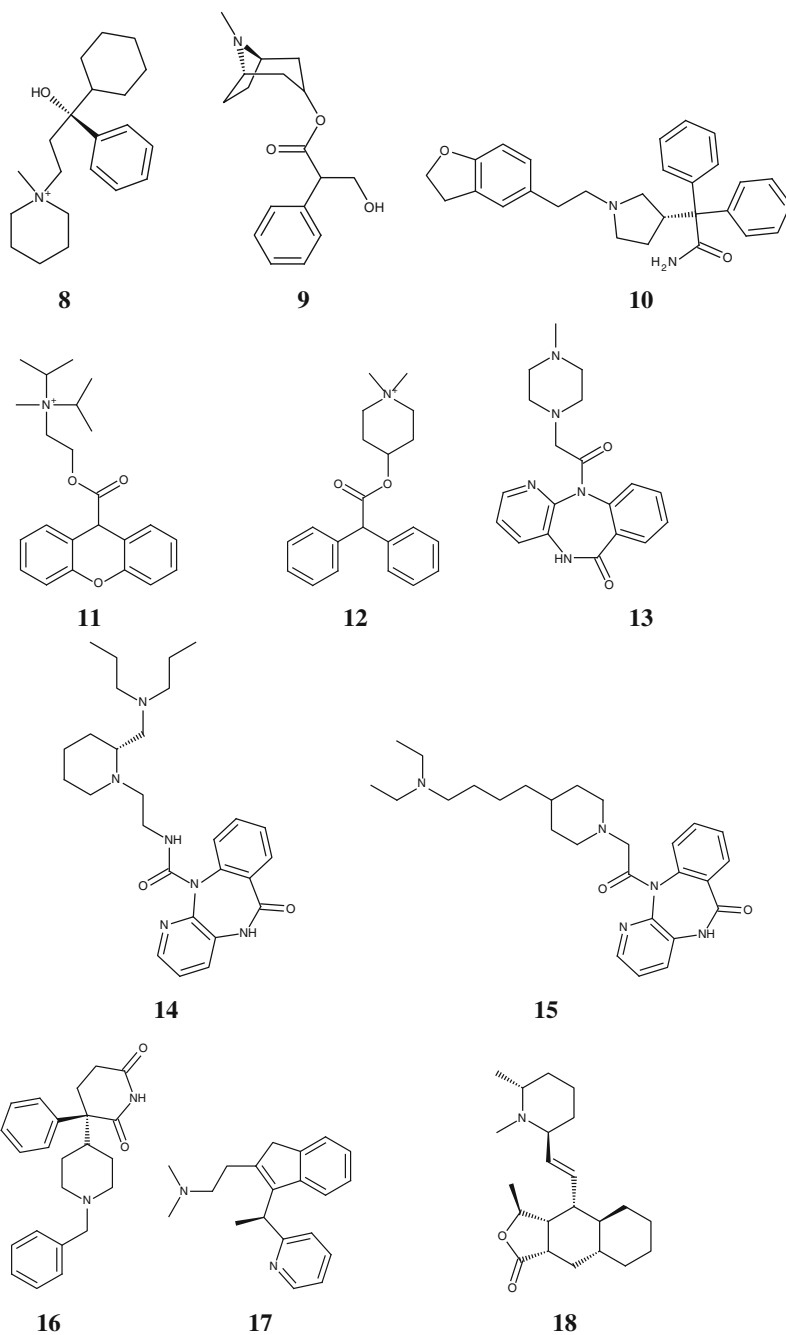


**Chart 11.1** Molecular structures of muscarinic receptor antagonists used for 3D pharmacophore elucidation

used for the docking studies of the known antagonists (Table 11.2) and the lactone derivatives (Table 11.1). Similar studies using M3 receptor were not performed despite the availability of the lone rat M3 receptor bound to an antagonist (PDB ID 4DAJ) [9].

The crystal structure of M2 receptor was prepared using protein preparation wizard. All the default settings were used in this step. Initial runs were performed using the crystal structure ligand, (3R)-1-azabicyclo[2.2.2]oct-3-yl hydroxy (diphenyl)acetate. The docking protocol using Extra Precision (Glide XP) outperformed the Standard Precision (Glide SP) mode with respect to the docking scores and reproduction of the binding mode of the crystal structure ligand (data not shown). Hence, for all the docking runs, Glide XP mode was used with default settings. The calculation of ligand binding energies was performed using MM-GBSA as implemented in Prime, version 3.2 [29]. All the default settings were used in this step.

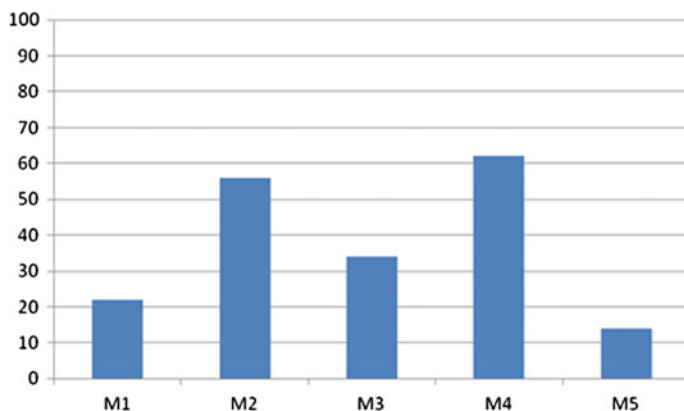
### 11.3 Results and Discussion

Table 11.1 represents the preliminary binding data of test compounds at a single concentration of 10  $\mu\text{M}$  and is presented as the percent inhibition of specific binding of radioligand.

Homologation approach caused an increase in affinity for each of the homologs tested. Affinity was influenced by the substitution pattern on the aromatic rings of the test compounds, but the case was not seen with the electronic nature of the substituents. For example, the unsubstituted compounds **9a** and **9b** inhibited specific binding by 16 and 74 %, respectively, while in the case of electron donating (**3a**, **3b**; **5a**, **5b**) and electron withdrawing (**7a**, **7b**; **8a**, **8b**) compounds, the ethylene series **3b** (56 %), **5b** (61 %), **7b** (57 %), and **8b** (70 %) showed higher percentage of specific inhibition (Table 11.1) regardless of the electronic nature of the substituent.

The para substituted compounds were similar to or less in their ability to inhibit specific binding over unsubstituted **9b**. Ortho substitution (**1a**, **1b**, **4a**, **4b**, **6a**, and **6b**) shows a similar pattern with their ethylene **1b** (82 %), **4b** (81 %), and **6b** (83 %) exhibiting higher % inhibition than their parent lactones regardless of the nature of the substituent. However, the ortho substitution was found to favor slightly higher % inhibition values than the corresponding unsubstituted **9b**, suggesting that ortho substitution may be preferred to para. A probable reason could be the influence of the ortho substitution on the orientation of the aromatic ring with respect to piperazine that may have affected the improvement in percentage inhibition values over other positions. Several additional piperazine-based derivatives (**10a**, **10b**, **11a**, **11b**, **15b**) were prepared and evaluated. In our former work, **11a** was found to have a high percentage inhibition value and was chosen for further evaluation ( $\text{IC}_{50} = 340 \text{ nM}$ ). Its homolog, **11b** showed the highest percentage inhibition and was chosen for further evaluation. The  $\text{IC}_{50}$  value (nonselective) for





**Fig. 11.3** Subtype selectivity data for hM<sub>1</sub>-hM<sub>5</sub> for compound **11b**

**11b** was found to be 17 nM, the highest affinity of any of the lactone-based muscarinic ligands reported to date. Compound **11b** was evaluated for its possible subtype selectivity due to its high affinity in the general muscarinic binding assay (see Fig. 11.3). Compound **11b** was tested at a concentration of 10 nM for its subtype selectivity on muscarinic receptor subtypes hM<sub>1</sub>-hM<sub>5</sub> and the values were found to be 22, 56, 34, 62, and 14 % for hM<sub>1</sub>-hM<sub>5</sub>, respectively, indicating no subtype selectivity exhibited for the compound.

In order to gain insights into the structural requirements of mAChR antagonists for potency and selectivity, 3D pharmacophore hypotheses and molecular docking investigations were conducted. Despite intensive research in this field, the design and development of selective antagonists for mAChR subtypes still remains a challenging task. The structural homology of the mAChRs in the orthosteric binding site seems to be the major obstacle.

### 11.3.1 3D Pharmacophore Elucidation

The first part of the study was initiated with the derivation of the 3D pharmacophore hypotheses for both the M<sub>1</sub>- and M<sub>2</sub> receptor antagonists. Since the majority of the known antagonists have mixed binding profiles at the mAChRs, we focused only on the M<sub>1</sub> and M<sub>2</sub> receptors. A careful inspection of the antagonists listed in IUPHAR database [30, 31] under M<sub>1</sub>-M<sub>5</sub> ligands section did not yield suitable hits which exhibited preferential selectivity for a particular mAChR. Hence, few hits from this database and some other literature reports [32, 33] constituted the final list of structurally diverse M<sub>1</sub>- and M<sub>2</sub>-preferring antagonists (Chart 11.1).

Compounds **8-13** were used for M<sub>1</sub> and compounds **9** and **14-18** were used for M<sub>2</sub> pharmacophore elucidation. The differences in pK<sub>i</sub> values for both the sets were in the 0–2 range, indicating that the antagonists were less than 100-fold selective for

either M1- or M2 receptors. Atropine was included in both the sets since it is a potent and nonselective antagonist and it represented the tropine derivatives class. The ranges of common molecular properties of the M1 set were—molecular weight (MW): 289.37–426.55; polar surface area (PSA): 23.47–68.78 Å<sup>2</sup>; H-bond acceptors (HBA): 1–3; H-bond donors (HBD): 0–1; rotatable bonds (RB): 2–7 and AlogP: 1.68–4.53. The corresponding values for the M2 set were—MW: 289.37–478.63; PSA: 16.13–80.81 Å<sup>2</sup>; HBA: 1–3; HBD: 0–2; RB: 2–9 and AlogP: 1.72–4.88.

The 3D pharmacophore hypotheses generation, scoring, clustering and careful inspection of the top two clusters led to the identification of common pharmacophoric features located at varied distances. The differences could be attributed to the conformational flexibility of the antagonists used in the present study. Figures 11.4 and 11.5 show the pharmacophore hypotheses developed using M1 and M2 antagonists, respectively. The features were mapped onto one of the antagonists used for the pharmacophore development process. For ease of understanding, these were termed as ‘extended’ and ‘compact’ (Fig. 11.6) hypotheses.

**Fig. 11.4** 3D pharmacophore hypotheses APR (A acceptor, P positive ionisable, R ring) for M1 receptor antagonists with corresponding feature alignment onto **a** compound **11** (propranolol, ball-and-stick model) and **b** **12** (4-DAMP, ball-and-stick model). The interfeature distances are shown for comparison

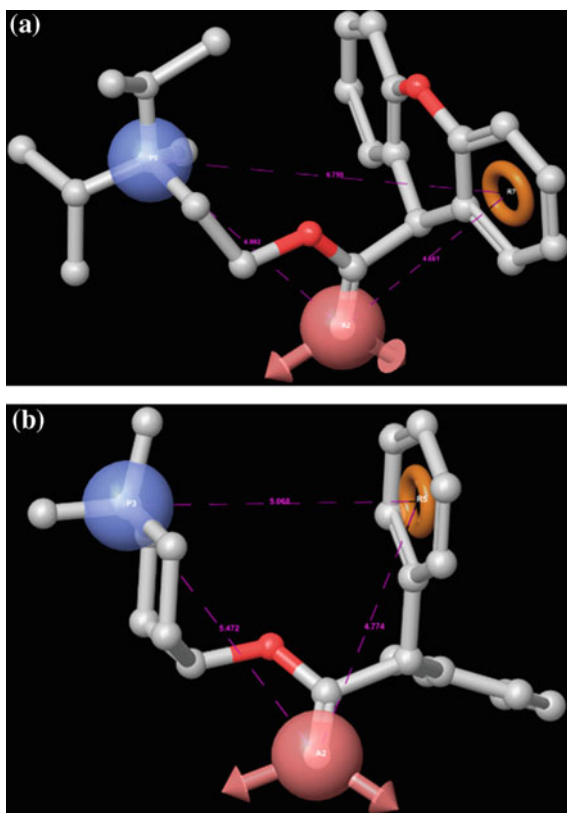


**Fig. 11.5** 3D pharmacophore hypotheses APR (A acceptor, P positive ionisable, R ring) for M2 receptor antagonists with corresponding feature alignment onto **a** compound **17** (*S*-dimethindene, ball-and-stick model) and **b** **16** (dexetimide, ball-and-stick model). The interfeature distances are shown for comparison

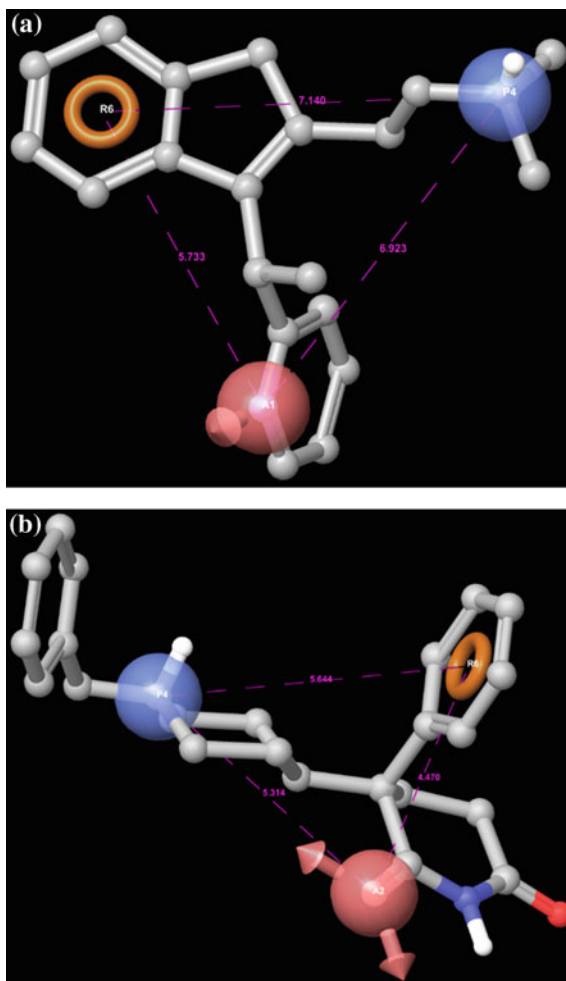
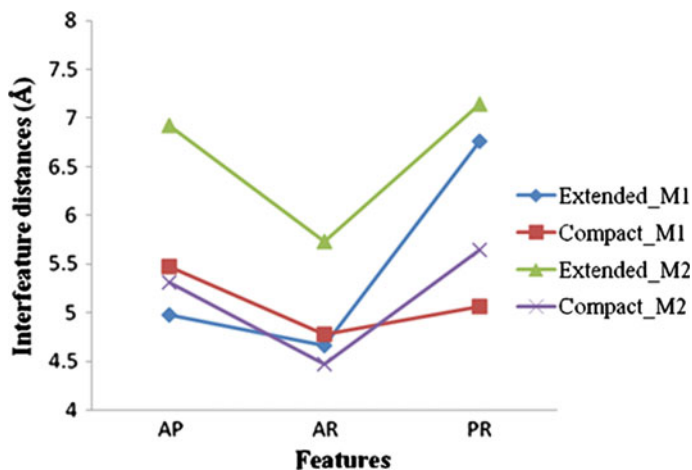


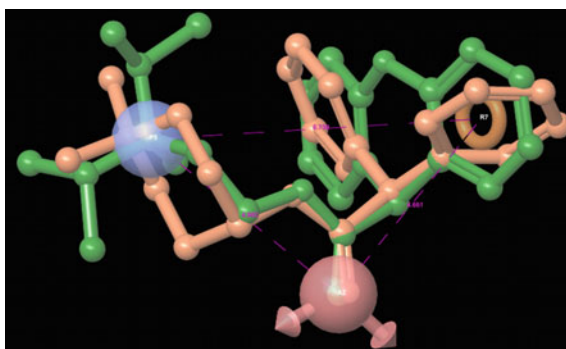
Figure 11.6 exhibits the interfeature distances against respective feature pairs—AP (acceptor-positive), AR (acceptor-ring) and PR (positive ring) for both the extended and compact M1 and M2 antagonist pharmacophore hypotheses. Careful examination of Fig. 11.6 showed that the hypotheses for M1 antagonists differed significantly in the PR distance (1.691 Å) while both the AP and AR distances were close enough. For M2 hypotheses, the differences in interfeature distances were relatively higher than the corresponding distance differences for M1 antagonists [AP (1.609 Å) > PR (1.496 Å) > AR (1.263 Å)], indicating possibly higher conformational flexibility of the M2 antagonists.

Compound **11** was found to be the best fit for the ‘extended’ whereas **12** appeared as the best fit for the ‘compact’ M1 hypotheses. This is in agreement to the



**Fig. 11.6** Interfeature distances plotted against feature pairs—AP, AR and PR—for extended and compact pharmacophore hypotheses (M1 and M2)

**Fig. 11.7** Alignment of **11** and **12** (ball-and-stick models) with corresponding mapping onto the M1 extended 3D pharmacophoric features. Compound **11** is shown in *green* while **12** is seen in *pink*



no. of rotatable bonds present (seven in **11** vs. five in **12**). Compound **13** was found to exhibit moderate fitness for both the hypotheses with higher relative energy for the extended version (data not shown). In other words, **13** was a better match for the compact M1 hypothesis. This is no surprise since the no. of rotatable bonds in **13** is only two. The alignments of **11** and **12** matching both the M1 hypotheses are shown in Figs. 11.7 and 11.8.

For M2 hypothesis, compound **18** was not considered by the software since it lacked the aromatic ring (R) feature. No further attempts were made to modify the feature definitions as implemented in Phase version 3.5 to accommodate **18**. The highest differences in the fitness values for the two hypotheses (extended and compact) were found for **16** and **17**, which were the best fit for the compact and extended hypotheses, respectively (data not shown). Alternatively, the best fit for one hypothesis was the lowest for the other. This observation may tap critical information in terms of subtle differences exhibited by these antagonists in their

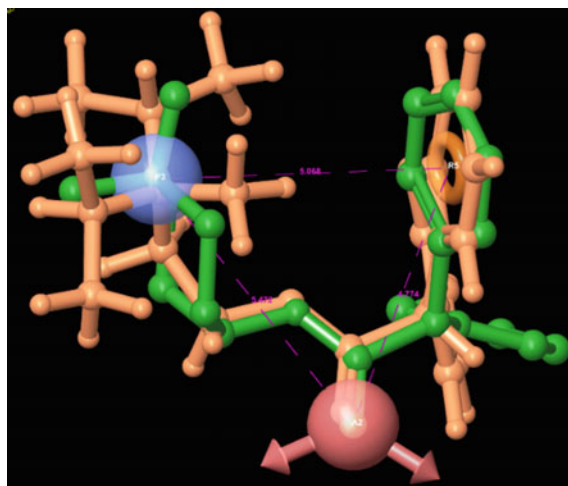


**Fig. 11.8** Alignment of **11** and **12** (ball-and-stick models) with corresponding mapping onto the M1 compact 3D pharmacophoric features. Compound **11** is shown in *pink* while **12** is seen in *green*

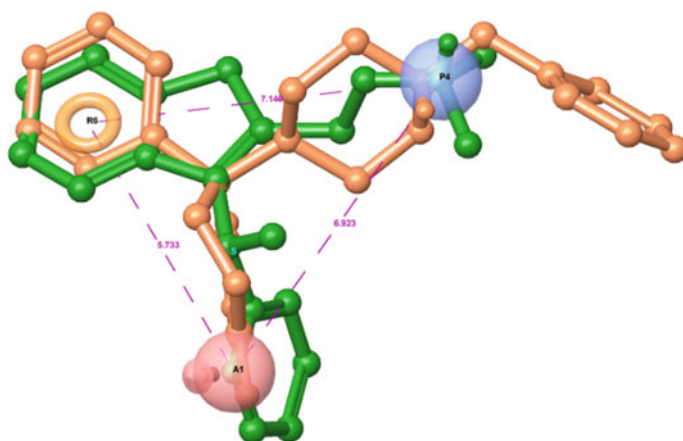
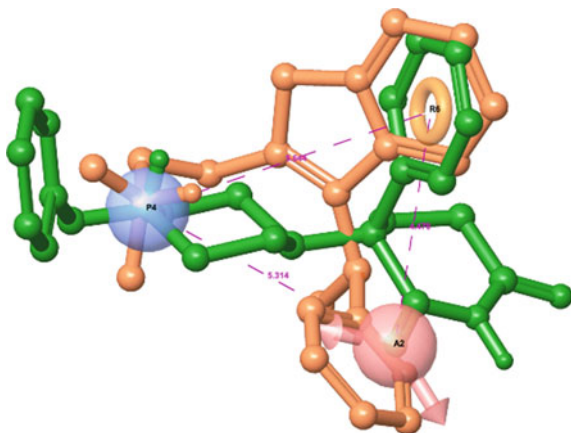


**Fig. 11.9** Alignment of **16** and **17** (ball-and-stick models) with corresponding mapping onto the M2 extended 3D pharmacophoric features. Compound **16** is shown in *pink* while **17** is seen in *green*

mAChR binding profiles. The extended M2 hypothesis stood apart from other M1 and M2 counterparts with respect to interfeature distances (Fig. 11.6). The alignments of **16** and **17** matching both the M2 hypotheses are shown in Figs. 11.9 and 11.10, respectively.

**Fig. 11.10** Alignment of **16** and **17** (ball-and-stick models) with corresponding mapping onto the M2 compact 3D pharmacophoric features. Compound **16** is shown in pink while **17** is seen in green



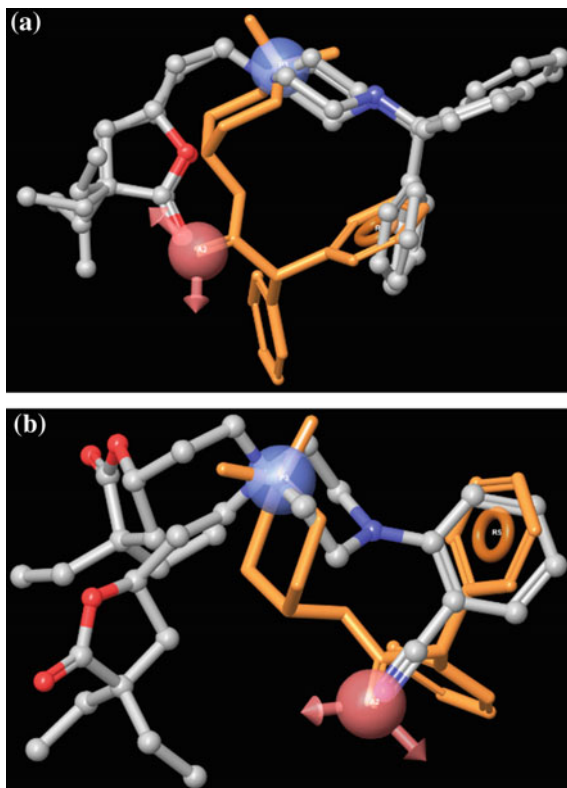
Compound **15** differed in the nature of the acceptor feature (pyridine N) from other antagonists (C=O oxygen as the acceptor feature). Overall, both the M1 and M2 antagonist hypotheses exhibited subtle differences in interfeature distances which may provide a clue for rationalizing their observed moderate/little selectivity, if any, for either of the two receptors.

### 11.3.2 Retrospective Virtual Screening of Lactone Derivatives

The lactone derivatives (Table 11.1) were used for virtual screening using the four pharmacophore hypotheses (M1/M2, extended/compact). Both the M1 hypotheses picked the compounds with two 'C' spacer ( $n = 2$ , Table 11.1) over those with one 'C' spacer ( $n = 1$ ). The hits common to both the hypotheses were **6b**, **10b**, **11b**, **13b**, and **15b**. This is in accordance with the SAR observation that the conformationally flexible derivatives ( $n = 2$ ) were more active than those with  $n = 1$  [22]. The alignment of **12** onto both the stereomers of **11b** with the corresponding mapping of the M1 compact hypothesis is seen in Fig. 11.11a. The acceptor feature was represented by the lactone 'C=O'. Compounds **1b**, **4b** and **6b** containing H-bond acceptor feature at the ortho position on the aromatic ring were among the top hits. The acceptor feature for these compounds was the ortho-substituent and not the lactone 'C=O'. Such compounds may exhibit profound differences in the potency and/or selectivity due to the altered nature and positions of the pharmacophoric features.

Similar to the M1 hypotheses-based virtual screening of the lactone derivatives, both M2 hypotheses selectively picked the two 'C' spacer ( $n = 2$ , Table 11.1) compounds over their methylene counterparts. Compounds **4b**, **5b**, **6b**, **9b**, **10b** and **13b** were present in both the hit lists.

**Fig. 11.11** M1 compact hypothesis with corresponding feature alignment onto compounds **a** (*R*)-**11b** and (*S*)-**11b** (ball-and-stick model), **b** (*R*)-**6b** and (*S*)-**6b** (ball-and-stick model). Compound **12** (orange capped-stick model) is shown for reference

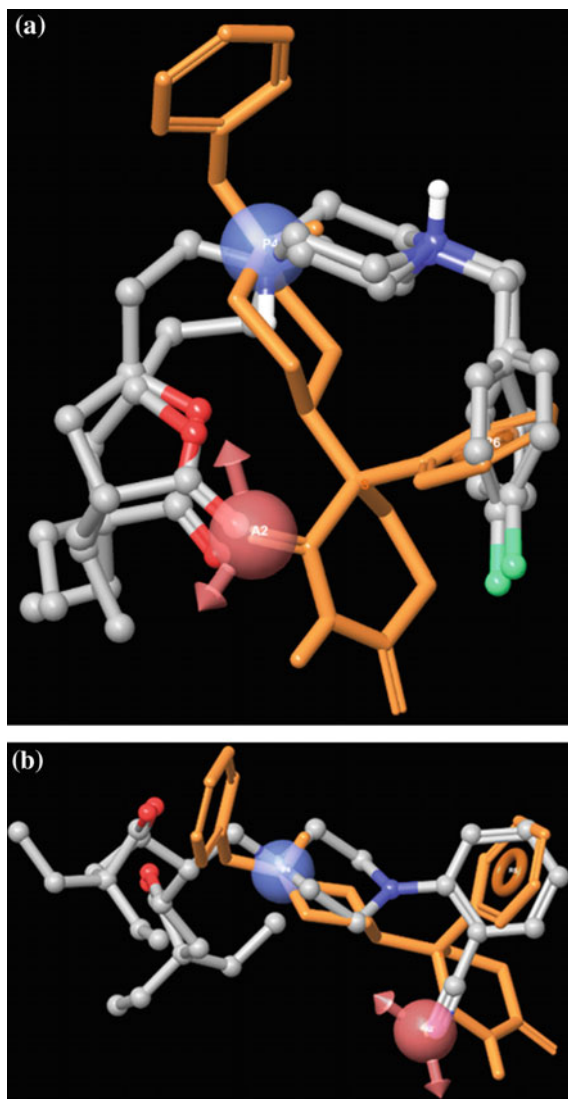


Lactone 'C=O' represents the acceptor feature in most of the compounds. A subset of the lactone derivatives in top hits contained ortho-substituent on the aromatic ring. In such compounds (e.g., **1b**, **4b** and **6b**), similar to M1 virtual screening hits, the acceptor feature was represented by the ortho-substituent as seen in Fig. 11.12b. Overall, the retrospective virtual screening of the lactone derivatives yielded interesting hits which were supported by the SAR. The hypotheses were able to pick active compounds from the collection. In view of the fact that the percentage inhibition values in Table 11.1 were derived from all mAChRs, the virtual screening results raised our confidence in the derived pharmacophore hypotheses for further design efforts.

### 11.3.3 Docking Studies

To further gain insights into the binding modes of the mAChR antagonists, molecular docking studies using the M2 receptor crystal structures were performed for the ligands used in the present investigation (Tables 11.1 and 11.2).

**Fig. 11.12** M1 compact hypothesis with corresponding feature alignment onto compounds **a** (*R*)-**10b** and (*S*)-**10b** (ball-and-stick model), **b** (*R*)-**6b** and (*S*)-**6b** (ball-and-stick model). Compound **16** (orange capped-stick model) is shown for reference



The docking scores and related parameters for all the ligands were calculated (data not shown). For quick reference, Glide XP GScore values of the known antagonists are given in Table 11.2. These values were found to correlate well with their corresponding M1 and M2  $pK_i$ s.

Figure 11.13 illustrates the binding mode of compound **9** (atropine) in the M2 receptor orthosteric binding site (PDB ID 3UON).

Most of the interactions including H-bonds formed by the crystal structure ligand with Asn404 (tropic acid) and Asp103 (cationic N) were observed for **9** as well. The binding modes of other ligands in Table 11.1 are shown in Figs. 11.14, 11.15, 11.16, 11.17, 11.18, 11.19, 11.20, and 11.21.



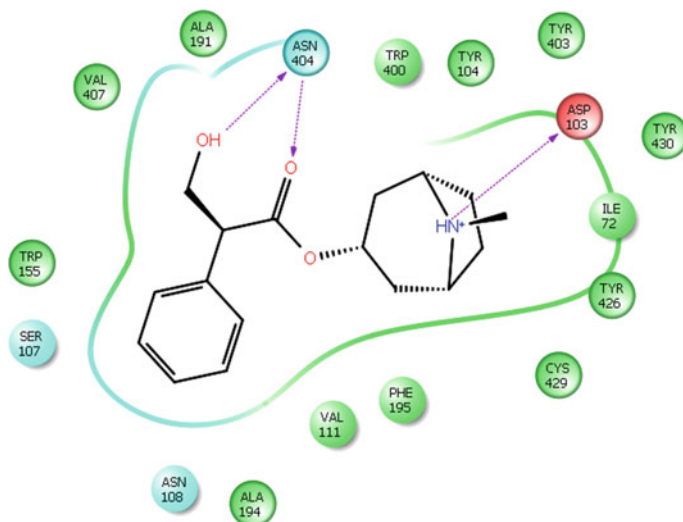


**Fig. 11.13** Binding mode of **9** in the antagonist-binding site of M2 receptor (PDB ID 3UON). The 2D ligand interaction diagram depicts the H-bonding, electrostatic and hydrophobic interactions of **9** with the M2 receptor

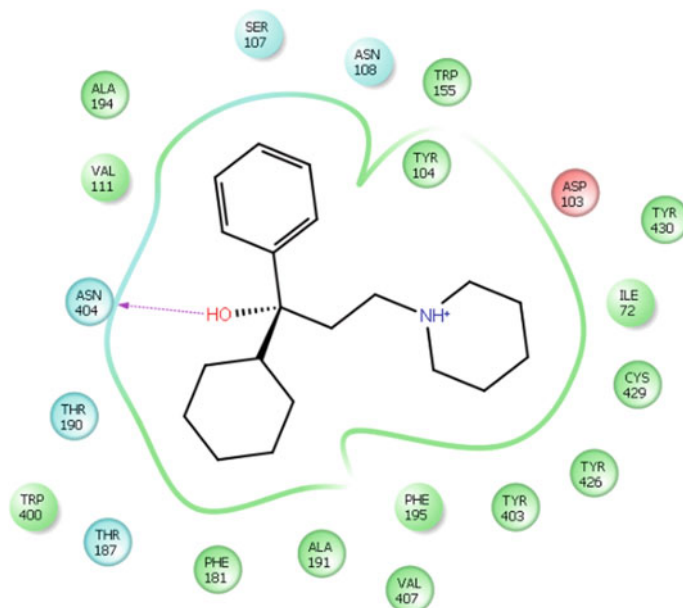


**Fig. 11.14** Binding mode of **8** in the antagonist-binding site of M2 receptor (PDB ID 3UON). The 2D ligand interaction diagram depicts the H-bonding, electrostatic and hydrophobic interactions of **8** with the M2 receptor

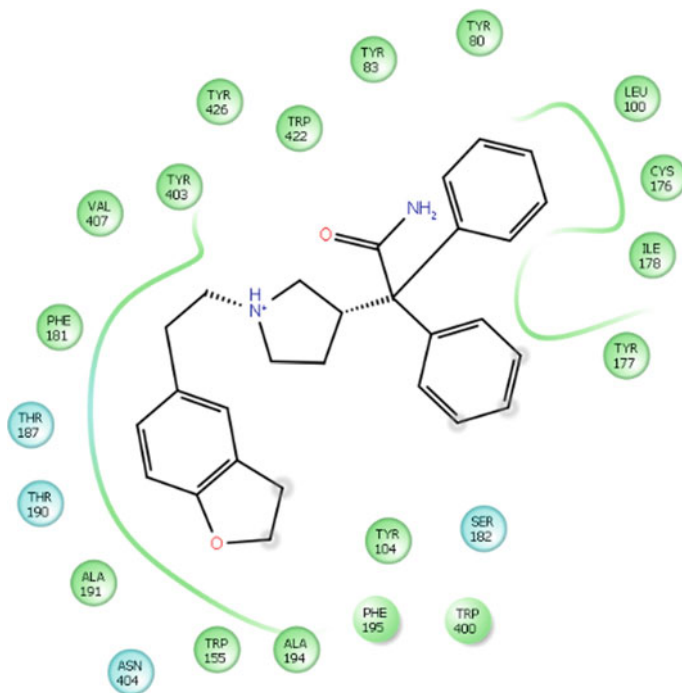


**Fig. 11.15** Binding mode of **10** in the antagonist-binding site of M2 receptor (PDB ID 3UON). The 2D ligand interaction diagram depicts the H-bonding, electrostatic and hydrophobic interactions of **10** with the M2 receptor

Further docking analyses of the lactone derivatives (**1a-15a** and **1b-15b**, Table 11.1) into the M2 receptor were carried out. Both the stereomers of each compound were docked. Of the two stereomers, for compounds **1a-15a** ( $n = 1$ , Table 11.1), *S*-isomers exhibited higher docking scores than the corresponding *R*-isomers (11 out of 15); for **1b-15b**, *R*-isomers exhibited higher docking scores than the corresponding *R*-isomers (11 out of 15). Since **1b-14b** were more potent than **1a-14a**, we carefully inspected the docking scores and the binding modes of all the compounds in order to derive important design hypotheses. The most potent compound **11b** (both stereomers) exhibited similar binding modes (Fig. 11.22) in the M2 orthosteric binding site. The lactone C=O formed H-bonds with Tyr426. No interaction was seen with Asp103. The docked poses of (*R*)-**11a** and (*R*)-**11b** are shown in Fig. 11.22. Only (*R*)-**11b** lactone C=O formed H-bond with Tyr426; lower homolog (*R*)-**11a** fell short of some distance to form H-bond with Tyr426.

This is in accordance with the observation that the ethylene spacer resulted in more potent compounds. The binding modes of compounds (*R*)-**9b** and (*R*)-**9a**, as seen in Fig. 11.23, clearly demonstrated that only (*R*)-**9b** was able to interact with Tyr426 whereas (*R*)-**9a** could not do so.

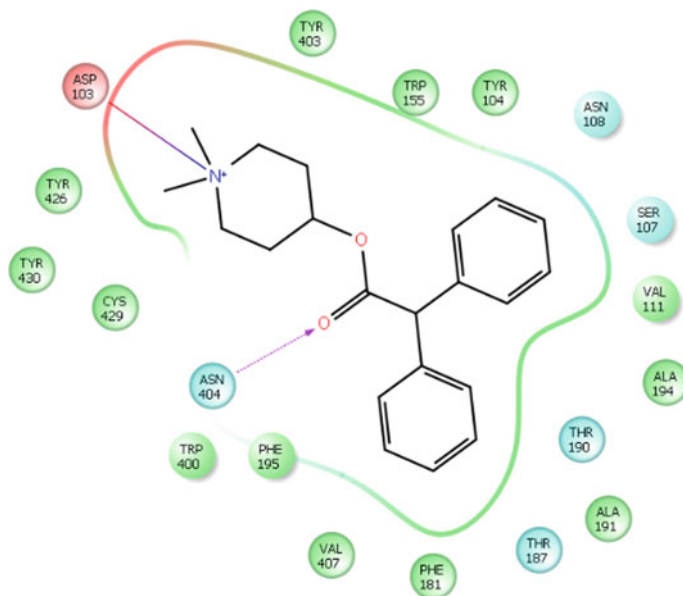


**Fig. 11.16** Binding mode of **12** in the antagonist-binding site of M2 receptor (PDB ID 3UON). The 2D ligand interaction diagram depicts the H-bonding, electrostatic and hydrophobic interactions of **12** with the M2 receptor

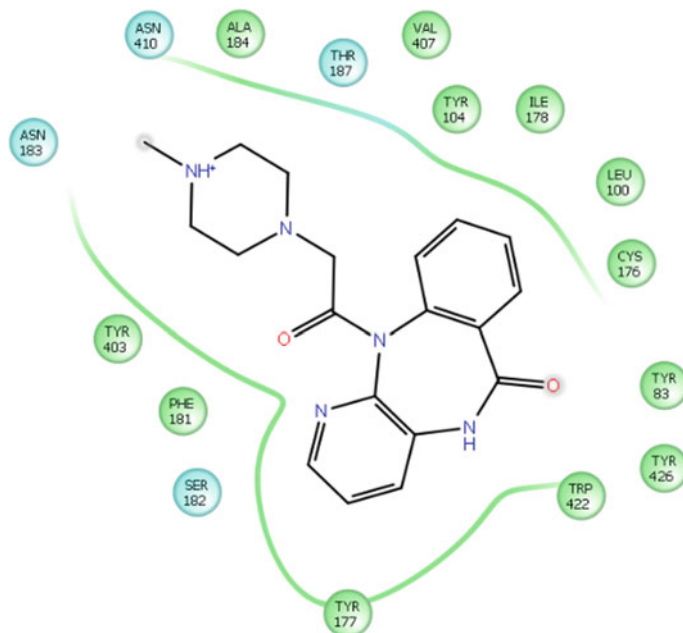


**Fig. 11.17** Binding mode of **13** in the antagonist-binding site of M2 receptor (PDB ID 3UON). The 2D ligand interaction diagram depicts the H-bonding, electrostatic and hydrophobic interactions of **13** with the M2 receptor

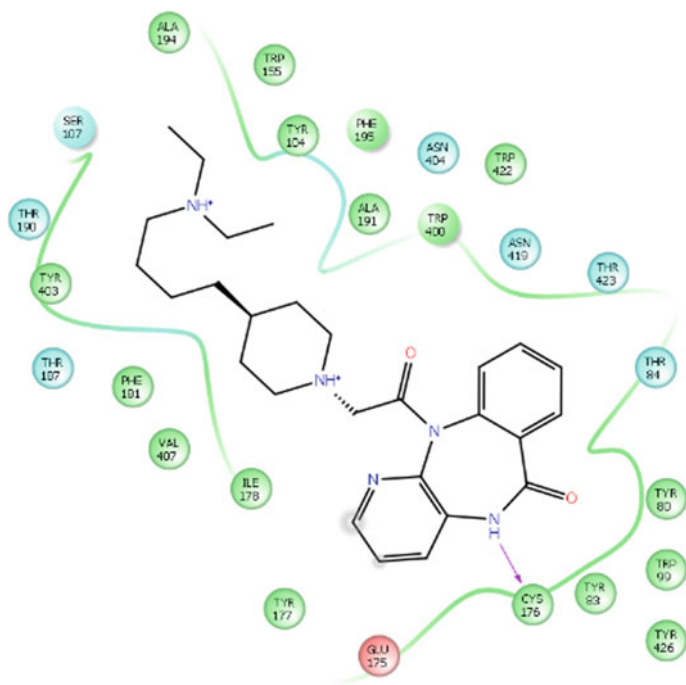


**Fig. 11.18** Binding mode of **15** in the antagonist-binding site of M2 receptor (PDB ID 3UON). The 2D ligand interaction diagram depicts the H-bonding, electrostatic and hydrophobic interactions of **15** with the M2 receptor

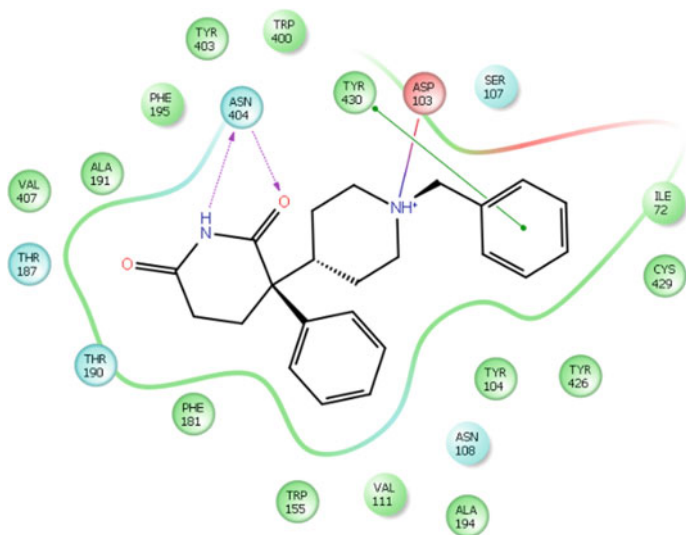


**Fig. 11.19** Binding mode of **16** in the antagonist-binding site of M2 receptor (PDB ID 3UON). The 2D ligand interaction diagram depicts the H-bonding, electrostatic and hydrophobic interactions of **16** with the M2 receptor

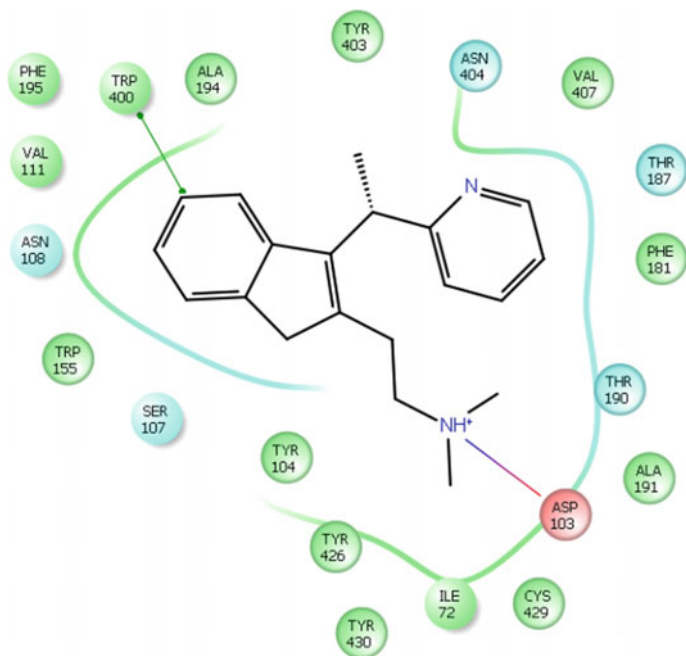


**Fig. 11.20** Binding mode of **17** in the antagonist-binding site of M2 receptor (PDB ID 3UON). The 2D ligand interaction diagram depicts the H-bonding, electrostatic and hydrophobic interactions of **17** with the M2 receptor

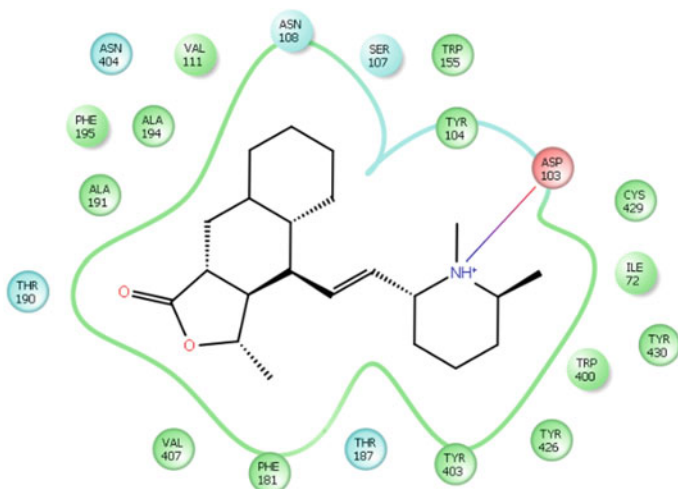


**Fig. 11.21** Binding mode of **18** in the antagonist-binding site of M2 receptor (PDB ID 3UON). The 2D ligand interaction diagram depicts the H-bonding, electrostatic and hydrophobic interactions of **18** with the M2 receptor

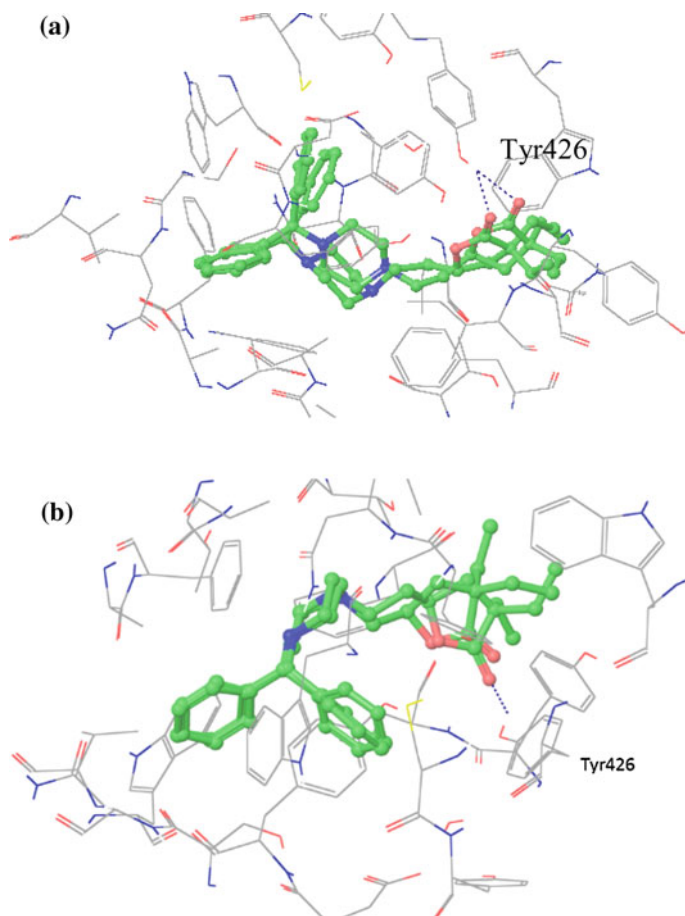


**Fig. 11.22** Binding modes of **a** (*R*)-11b and (*S*)-11b and **b** (*R*)-11a and (*R*)-11b in the antagonist-binding site of M2 receptor (PDB ID 3UON). The lactone C=O forms H-bonds with 4-OH of Tyr426

The binding energy computations using MM-GBSA led to interesting outcomes. A plot of percentage inhibition versus MM-GBSA  $dG$  binding (Fig. 11.24) clearly distinguished the methylene series ( $n = 1$ , Table 11.1) from the homologous ethylene series. This further strengthened our belief in the observed binding modes and the critical information obtained therein.

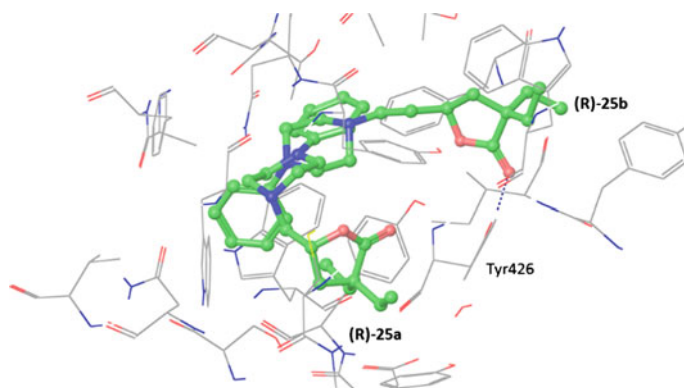


**Fig. 11.23** Binding modes of (R)-9a and (R)-9b in the antagonist-binding site of M2 receptor (PDB ID 3UON). The lactone C=O of (R)-9b forms H-bond with Tyr426

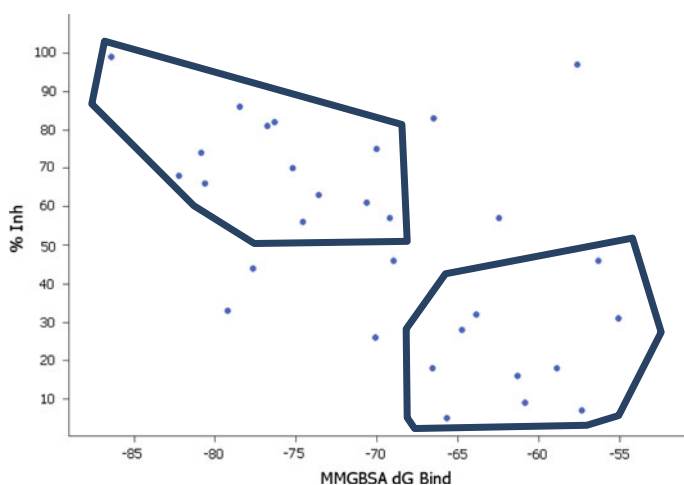


**Fig. 11.24** Plot of percentage inhibition (at 10  $\mu$ M) versus MM-GBSA dG binding. The shapes clearly divide the two series—methylene ( $n = 1$ ) and ethylene ( $n = 2$ )—based on their binding energy and percentage inhibition. Ethylene series is located in the *upper left-hand corner* and the methylene series is seen at the *lower right hand corner*

## 11.4 Conclusions

In summary, the present work describes the combined utilization of the ligand-based (pharmacophore elucidation for M1- and M2-receptor antagonists) and structure-based (docking analyses of the known antagonists and lactone derivatives) approaches, followed by retrospective virtual screening of the lactone derivatives which helped us to understand the critical design parameters. These

studies demonstrated the successful application of the ligand- and structure-based approaches for the design of novel muscarinic ligands with more emphasis on receptor subtype selectivity.

**Acknowledgements** RB and PK thank Dr. R.S. Gaud, Dean, SPP School of Pharmacy and Technology Management, SVKM's NMIMS, Mumbai, India, for his constant support and encouragement during preparation of this book chapter.

## References

1. Karnik SS, Gogonea C, Patil S, Saad Y, Takezako T (2003) Activation of G-protein-coupled receptors: a common molecular mechanism. *Trends Endocrinol Metab* 14:431–437
2. Scarselli M, Li B, Kim SK, Wess J (2007) Multiple residues in the second extracellular loops are critical for M3 muscarinic acetylcholine receptor activation. *J Biol Chem* 282:7385–7396
3. Hosey MM (1992) Diversity of structure, signaling and regulation within the family of muscarinic cholinergic receptors. *FASEB J* 6:845–852
4. Wess J, Eglén RM, Gautam D (2007) Muscarinic acetylcholine receptors: mutant mice provide new insights for drug development. *Nat Rev Drug Discov* 6:721–733
5. Chan WY, McKinzie DL, Bose S, Mitchell SN, Witkin JM, Thompson RC, Christopoulos A, Lazareno S, Birdsall NJM, Bymaster FP (2008) Allosteric modulation of the muscarinic M4 receptor as an approach to treating schizophrenia. *Proc Natl Acad Sci* 105:10978–10983
6. Felder CC, Bymaster FP, Ward J, DeLapp N (2000) Therapeutic opportunities for muscarinic receptors in central nervous system. *J Med Chem* 43:4333–4353
7. Felder CC (1995) Muscarinic acetylcholine receptors: signal transduction through multiple effectors. *FASEB J* 9:619–625
8. Haga K, Kruse AC, Asada H, Yurugi-Kobayashi T, Shiroishi M, Zhang C, Weis WI, Okada T, Kobilka BK, Haga T, Kobayashi T (2012) Structure of the human M2 muscarinic acetylcholine receptor bound to an antagonist. *Nature* 482:547–551
9. Kruse AC, Hu J, Pan AC, Arlow DH, Rosenbaum DM, Rosemond E, Green HF, Liu T, Chae PS, Dror RO, Shaw DE, Weis WI, Wess J, Kobilka BK (2012) Structure and dynamics of the M3 muscarinic acetylcholine receptor. *Nature* 482:552–556
10. Kuduk SD, Beshore DC (2012) Novel M1 allosteric ligands: a patent review. *Expert Opin Ther Pat* 22:1385–1398
11. Dror RO, Green HF, Valant C, Borhani DW, Valcourt JR, Pan AC, Arlow DH, Canals M, Lane JR, Rahmani R, Baell JB, Sexton PM, Christopoulos A, Shaw DE (2013) Structural basis for modulation of a G-protein-coupled receptor by allosteric drugs. *Nature* 503:295–299
12. Kruse AC, Ring AM, Manglik A, Hu J, Hu K, Eitel K, Hübner H, Pardon E, Valant C, Sexton PM, Christopoulos A, Felder CC, Gmeiner P, Steyaert J, Weis WI, Garcia KC, Wess J, Kobilka BK (2013) Activation and allosteric modulation of a muscarinic acetylcholine receptor. *Nature* 504:101–106
13. Thomas T, McLean K, McRobb FM, Manallack DT, Chalmers DK, Yuriev E (2013) Homology modeling of human muscarinic acetylcholine receptors. *J Chem Inf Model* 54:243–253
14. Bhattacharjee AK, Pomponio JW, Evans SA, Pervitsky D, Gordon RK (2013) Discovery of subtype selective muscarinic receptor antagonists as alternatives to atropine using in silico pharmacophore modeling and virtual screening methods. *Bioorg Med Chem* 21:2651–2662
15. Pedretti A, Vistoli G, Marconi C, Testa B (2006) Muscarinic receptors: a comparative analysis of structural features and binding modes through homology modelling and molecular docking. *Chem Biodiver* 3:481–501



16. Marriott DP, Dougall IG, Meghani P, Liu YJ, Flower DR (1999) Lead generation using pharmacophore searching: application to muscarinic M3 receptor antagonists. *J Med Chem* 42:3210–3216
17. Peng JY, Vaidehi N, Hall SE, Goddard WA (2006) The predicted 3D structures of human M1 muscarinic acetylcholine receptor with agonist or antagonist bound. *ChemMedChem* 1:878–890
18. Johnen K, Holtje HD (2002) A model of human M2 muscarinic acetylcholine receptor. *J Comput Aided Mol Des* 16:795–801
19. Ostopovici L, Mracec M, Mracec M, Borota A (2007) Exploring the binding site of human muscarinic M3 receptor: homology and docking study. *Int J Quantum Chem* 07:1794–1802
20. Ahungena A, Gabriel JL, Canney DJ (2003) Synthesis and evaluation of 5-substituted derivatives of 4,5-dihydro-3,3-diethyl-2(3H)-furanone as subtype-selective muscarinic leads. *Med Chem Res* 12:481–511
21. Kaiser C, Spagnuolo CJ, Adams TC, Audia VH, Dupont AC, Hatoum H, Lowe VC, Prosser JC, Sturm BL, Noronha-Blob L (1992) Synthesis and antimuscarinic properties of some N-substituted 5-(aminomethyl)-3,3-diphenyl-2(3H)-furanones. *J Med Chem* 35:4415–4424
22. Bhandare RR, Canney DJ (2011) Modifications to five-substituted 3,3-diethyl-4,5-dihydro-2(3H)-furanones en route to novel muscarinic receptor ligands. *Med Chem Res* 20:558–565
23. Schrödinger Small-Molecule Drug Discovery Suite Release 2013-1 (2013) is available from Schrödinger, LLC, New York
24. Phase, version 3.5, Schrödinger (2013) LLC, New York
25. Maestro, version 9.4, Schrödinger (2013) LLC, New York
26. LigPrep, version 2.6, Schrödinger (2013) LLC, New York
27. Dixon SL, Smondyrev AM, Knoll EH, Rao SN, Shaw DE, Friesner RA (2006) Phase: a new engine for pharmacophore perception, 3D QSAR model development, and 3D database screening. 1. Methodology and preliminary results. *J Comput-Aided Mol Des* 20:647–671
28. Glide, version 5.9, Schrödinger (2013) LLC, New York
29. Prime, version 3.2, Schrödinger (2013) LLC, New York
30. Birdsall NJM, Brown DA, Buckley NJ, Christopoulos A, Eglen RM, Ehlert F, Hammer R, Kilbinger HJ, Lambrecht G, Mitchelson F, Mutschler E, Nathanson NM, Schwarz RD, Tobin AB, Wess J (2013) Acetylcholine receptors (muscarinic): M1 receptor. IUPHAR database (IUPHAR-DB), <http://www.iuphar-db.org/DATABASE/Object-displayForward?objectId=13>. Last modified on 24 Sept 2013. Accessed on 08 Jan 2014
31. Birdsall NJM, Brown DA, Buckley NJ, Christopoulos A, Eglen RM, Ehlert F, Hammer R, Kilbinger HJ, Lambrecht G, Mitchelson F, Mutschler E, Nathanson NM, Schwarz RD, Tobin AB, Wess J (2013) Acetylcholine receptors (muscarinic): M2 receptor. IUPHAR database (IUPHAR-DB), <http://www.iuphar-db.org/DATABASE/ObjectDisplayForward?objectId=14>. Last modified on 09 Dec 2013. Accessed on 08 Jan 2014
32. Dorje F, Wess J, Lambrecht G, Tacke R, Mutschler E, Brann MR (1991) Antagonist binding profiles of five cloned human muscarinic receptor subtypes. *J Pharm Exp Therap* 256:727–733
33. Pfaff O, Hildebrandt C, Waelbroeck M, Hou X, Moser U, Mutschler E, Lambrecht G (1995) The (S)-(+)-enantiomer of dimethindene: a novel M2-selective muscarinic receptor antagonist. *Eur J Pharmacol* 286:229–240